Computational Fluid Dynamics Based Approach for Predicting Heat Transfer and Flow Characteristics of Inline Tube Banks with Large Transverse Spacing

Niko Pietari Niemelä, Antti Mikkonen, Kaj Lampio, Jukka Konttinen

Materials Science and Environmental Engineering, Tampere University, Kalevantie 4, 33100 Tampere, Finland

Address correspondence to Niko Pietari Niemelä, Tampere University (TAU), Kalevantie 4, 33100 Tampere, Finland, E-mail: niko.niemela@tuni.fi, Phone Number: +358 40 838 1434

ABSTRACT

Inline tube configuration is used in various heat exchangers, such as power plant superheaters. The important design parameters are the longitudinal and transverse spacing between the tubes, as they determine the flow and heat transfer characteristics of the tube bank. In superheaters, the transverse tube spacing is often relatively large in order to avoid clogging of the flow passages due to deposition of particulate matter. To design and optimize superheaters is a challenging task, especially because of the complicated vortex-shedding phenomenon. This also complicates the Computational Fluid Dynamics (CFD) modeling, because unsteady simulation approach is required. This paper discusses about various factors that affect the accuracy of prediction of heat transfer and flow characteristics of inline tube banks with large transverse spacing. A suitable CFD model is constructed by comparing different boundary conditions, domain dimensions, domain size, and turbulence models in unsteady simulations. The numerically obtained Nusselt numbers are evaluated against available heat transfer correlations. The correlation of Gnielinski is recommended for tube banks with large transverse spacing, as it agrees within ±13% with the numerically obtained values. The guidelines presented in the paper can serve as reference for future simulations of unsteady flow phenomena.

INTRODUCTION

Inline tube configuration is widely used in numerous heat transfer applications, such as in power plant superheaters. In power plants, the particulate matter carried by the flue gas can deposit on the superheater surfaces and cause clogging of the flow passages. To avoid this, the transverse spacing S_T of the tube columns is usually designed relatively large. In this work, inline tube banks with large transverse spacing are studied numerically with Computational Fluid Dynamics (CFD). A CFD based approach is presented, which can address important design questions and give detailed information related to flow characteristic and heat transfer in superheater tube banks.

Inline tube banks have been widely studied by both experimental and numerical means. Zukauskas [1] has developed a widely used heat transfer correlation for varying tube spacing. Since their work, multiple correlations have been developed such as the correlations of Gnielinski [2] and Martin [3]. However, all of these correlations have been mostly fitted to experimental data for compact tube banks, where the transverse pitch ratio is in the range $a = S_T/D < 3$. Little information can be found regarding accuracy above this range, even though the flue gas side heat transfer coefficient has a large impact on the overall heat transfer predictions and is thus an important parameter of detailed mathematical models and simulations of superheater systems, see [4-6]. In this work, the available correlations are evaluated against numerical simulations in the transverse pitch ratio range $1.8 \leq a \leq 7.2$, in order to find the most suitable correlation for evaluating the convective heat transfer in the flue gas side of superheaters.

Von Karman type flow oscillations are characteristic for inline tube banks and are an important design factor to take into consideration. The oscillations can cause tube vibrations and generate excessive acoustic noise in the flow channels, posing challenges to the dimensioning of the tube banks. Many authors have conducted experimental studies and developed Strouhal

number charts, which can be used for calculating the critical flow velocity where vibration problems may occur, see [7, 8]. Ziada [9] has reported a large number of experiments and flow visualizations for vortex shedding in various tube bank geometries. The oscillations have been studied also numerically for tube banks with different number of tubes [10-12]. Again, the majority of the studies have concerned compact tube bank geometries. Therefore, the oscillation characteristics and Strouhal numbers for large transverse spacing are analyzed in this work.

In recent years, together with the rapid increase of computational resources, the numerical CFD analysis of flow and heat transfer in tube banks has increased. The recent publications are trending towards Large Eddy Simulation (LES), which has become a widely used tool in academic CFD studies also for tube banks [13-15]. Compared to the Reynolds-Averaged Navier-Stokes (RANS) methodology, the LES simulations consume significantly more CPU time, and thus, are not practical for industrial research and development. The RANS methodology is currently the industrial standard, but its suitability especially for unsteady simulations (URANS) has been debated in the CFD field. Unsteady flow separation, such as in the inline tube banks, is traditionally considered the weakness of RANS type turbulence modelling. However, the studies of Iaccarino et al. [16] and Elkhoury [17] show that URANS methodology is capable of predicting the main flow characteristics also in this kind of complex flows. Both of these studies analyze a square cylinder in cross flow, and show that the Strouhal number and length of the separation bubble can be reasonably well predicted with URANS approach, if compared to experimental data and LES simulations. In the present study, the URANS simulations are further analyzed, as the inline tube banks with large transverse spacing pose an even more challenging flow problem compared to a single square cylinder. Multiple state-of-the-art turbulence models are examined, including two types of Reynolds Stress Model (RSM), Scale Adaptive Simulation (SAS) and k-ω SST model.

THEORETICAL BASIS AND MODEL DESCRIPTION

The different tube bank geometries analyzed in the CFD simulations are presented in Fig. 1 (labelled with letters from A to E). The transverse pitch ratio $a = S_T/D$ and longitudinal pitch ratio $b = S_L/D$ are varied from 1.8 to 7.2 and 1.5 to 2.7, respectively. Two standard tube outer diameters D are used in the simulations (63.5 and 44.5 mm).

The velocity in the free flow channel before the tube bank is $U_\infty = 5$ m/s in most simulations. This velocity represents a typical value in superheater flow channels. The Reynolds number and Nusselt number used throughout this paper are defined using the tube bank void fraction $\Psi = 1 - \pi/(4a)$ and the streamed tube length $l = \pi D/2$, as follows:

$$\mathrm{Re}_{\Psi,l} = \frac{U_\infty l}{\Psi \nu} \quad ; \quad \overline{\mathrm{Nu}_l} = \frac{\bar{h} l}{k} \qquad (1)$$

These definitions are used for being consistent with the heat transfer correlation of Gnielinski [2].

The mean convective heat transfer coefficient $\bar{h}$ for the tube bank is calculated from the CFD results as:

$$\bar{h} = \frac{\bar{\dot{Q}}}{A \Delta T_{lm}} \qquad (2)$$

where $\bar{\dot{Q}}$ (W) is the convective heat transfer rate of the domain tubes time-averaged over at least ten oscillation periods in the statistically stationary solution. ΔT_{lm} is the logarithmic mean temperature difference of the flue gas across the simulation domain and A is the total surface area of the tubes.

The simulation domains used in this work are presented in Fig. 2. The periodic domain (a) has a width of S_T, a length in the flow direction of $5S_L$, and a height of three tube diameters. Five heat transfer tubes are included to ensure sufficient domain length in the main flow direction. Periodic boundary conditions are used in all domain boundaries unless otherwise stated. The two-

dimensional periodic simulations presented in the work are calculated with similar domain but with zero height. The results of larger 2D domain of 144 tubes (label (b) in Fig. 2) are compared to the periodic simulations. The large domain has periodic boundaries on the domain sides, constant inlet velocity and pressure outlet boundary conditions. All meshes used in this work have the first cell y^+ close to one and consist of hexahedral mesh elements. Sufficient mesh resolution for different simulation domains is reached by conducting a mesh independence study for geometry B and $\mathrm{Re}_{\Psi,l} = 5690$, results presented in Table 1.

Material properties and other constants for the simulations and heat transfer correlations are presented in Table 2. The properties are those for a flue gas containing N_2, O_2, CO_2 and H_2O in a temperature of 914 K, representing average temperature in a superheater. The tube surface temperature is constant at 612 K. Constant material properties are used, because temperature dependent values cannot be used with periodic boundary conditions in ANSYS Fluent 17.1.

The numerical CFD solutions are obtained with the Finite-Volume Method using commercial ANSYS Fluent 17.1 software [18], but also OpenFOAM [19] is examined for code comparison. The governing equations of fluid flow and heat transfer are described in fluid dynamics books. All simulations are conducted time-dependently with the domain maximum Courant number at approximately 0.6. The first order implicit scheme for time derivatives is used in 2D simulations, whereas the bounded second-order implicit scheme is used in 3D simulations. QUICK scheme is used for evaluating the cell face gradients for convective terms. URANS methodology is chosen for its reduced calculation time compared to LES. The turbulence closure problem is solved with multiple different turbulence models.

Two different types of 7-equation (5 eqs. in 2D) RSM's are evaluated. RSM is a closure model that solves transport equations for each independent Reynolds Stress, and thus is not based

on the Boussinesq hypothesis. The two formulations differ by treatment of the pressure-strain term and turbulent dissipation variable. The first model uses the Linear-Pressure-Strain formulation and solves ε as a variable for turbulent dissipation, labelled RSM-LPε in this work. The second model uses the Launder-Reese-Rodi formulation for pressure strain and solves ω to describe turbulent dissipation [18]. It treats the wall boundary layers similarly as the standard k-ω –model of Wilcox [20], and is labelled RSM-ω.

In addition to the RSM-models, the SST formulation of k-ω –model and the SAS are examined. The k-ω SST is a 2-equation turbulence model based on the Boussinesq hypothesis. It is known to be efficient for solving complex boundary layer flows. The SAS model, on the other hand, is a relatively new model and can be considered as URANS model with LES-like scale resolving capabilities. It keeps track of a turbulent length scale and adjusts the resolved turbulence structures during the solution procedure. In this work, the k-ω SST formulation of SAS is used. More information about all described models can be found in the ANSYS Fluent theory guide [18]. Only the k-ω SST model is used in OpenFOAM simulations.

The main equations for the analyzed heat transfer correlations are presented in Table 3. The correlation of Gnielinski [2] is recommended for inline tube banks in many heat transfer books, detailed description can be found in VDI Heat Atlas [21]. Zukauskas correlation is historically the oldest and still widely used, see description in [22]. Martin [3], on the other hand, has demonstrated the usefulness of the Leveque analogy for many types of heat exchangers. The Leveque analogy correlates the convective heat transfer rate to frictional pressure drop calculated from the correlation of Gaddis and Gnielinski [23]. The correlation is relatively new, but already recommended in some heat transfer books such as [24]. A shortcoming of Martin correlation [3]

is that is only recommended for transverse pitch ratios of $a \leq 3$, because of the validity range of Gaddis and Gnielinski pressure drop correlation [23].

RESULTS AND ANALYSIS

Effect of domain on CFD results

With large superheater tube banks, the choice of simulation domain is not trivial because numerous different possibilities exist. Simulation for a complete tube bank is not computationally feasible, because to ensure sufficient boundary layer mesh resolution with even moderate Re-numbers, the cell count rises very high already in 2D simulations. Because a tube bundle consists of a repeated pattern of tubes, it can be divided into smaller periodic or symmetric domains to save CPU time. Different approaches have been adopted, such as assuming the tube rows as hexahedral platens [25], simulating one gap between the tube rows using symmetry boundary conditions [26], or simulating only a few tubes using periodic boundary conditions [27]. The effect of simulation domain and boundary conditions on the CFD heat transfer predictions is analyzed in this section in order to clarify how the different choices affect the simulation results. Thus, the results can serve as reference for future studies where unsteady flow phenomena in tube banks is studied.

The analyzed factors here are the effect of domain dimensions (2D vs 3D), the effect of the domain size (large domain of 144 tubes versus vs periodic domain of 5 tubes) and the effect of boundary conditions (symmetry vs periodic). The results are presented in Fig. 3, which shows the typical time-varying heat flux signal for a single tube in the domain, calculated with the *k*-ω SST model. The domain dimensions do not significantly affect the heat transfer predictions (graph on the left), as both the 2D and the 3D domains predict the same time-average heat flux and oscillation frequency. However, the amplitude of the fluctuations is slightly higher in 2D simulation. The

similarity is surprising, as the 3D results show that there are significant velocities in the direction parallel to the tubes (Z-direction). The maximum Z-velocities in the domain are close to the free channel velocity $U_\infty = 5$ m/s. To demonstrate the three-dimensional nature of the flow field, the vortex structures and the local heat flux on the tube surfaces are demonstrated in Fig. 4 (SAS turbulence model). The figure indicates that the strongest 3D vortices develop after boundary layer separation from the tubes. The velocity field close to the tubes is more 2-dimensional, partly explaining the similarity of the 2D and 3D heat transfer predictions.

The graph on the right side of Fig. 3 shows that the choice of the boundary conditions has very large effect on the heat transfer predictions. Both simulations are calculated with periodicity in the flow direction, but in the symmetry case the domain sides are defined symmetric (see label (a) in Fig. 2), meaning the velocity gradients are zero and no flow goes through the boundary. The symmetry condition reduces the flow oscillations significantly and results in 20% weaker time-average heat transfer rate for the tubes. As seen later, the periodic simulations agree very well with the heat transfer correlations, thus indicating that symmetry boundaries are not recommended for tube bank simulations where significant oscillations occur. A larger domain with multiple tube columns might result in better predictions if symmetry conditions are used on the domain sides.

Fig. 5 shows the results for the larger simulation domain with 144 tubes in geometry B (see label (b) in Fig. 2) and $\mathrm{Re}_{\Psi,l} = 5690$. The simulation has been conducted with OpenFOAM solver using 2D domain and the *k*-ω SST model. The Fluent and OpenFoam codes were initially compared with small periodic domain, both giving the same Nusselt number within 0.5 % accuracy. As Fig. 5 indicates, the heat flux varies for different tube rows in the large domain, and a mean Nusselt number of 58.8 is obtained for the tube bundle. This is close to the value of 64.0 obtained with the small 2D periodic domain and very close to the heat transfer correlation of

Gnielinski [2] ($\overline{\mathrm{Nu}_l} = 58.7$). For more detailed comparison of the simulation domains, Fig. 6 shows the heat flux signals as a function of time for two tubes in the large domain (in rows 6 and 19) and for one tube in the small periodic domain. In the large domain, the heat flux signal for the tube in row 6 varies consistently in time, whereas for the tube in row 19 the signal becomes more chaotic. However, the Fast Fourier Transform (FFT) reveals nearly the same characteristic frequency for both tubes (20 Hz). The heat flux signal is very similar for the tube in the small periodic domain, confirmed by nearly the same characteristic frequency (23 Hz). The results indicate that the periodic simulation domain is able to predict the unsteady behavior of the tube bundle and provide useful information with considerable savings in the CPU time.

Comparison of Turbulence Models

The different turbulence models are compared in Fig. 7. The *k*-ω SST model is kept as a baseline model (solid lines) and the other models (dashed lines) are compared to its results. The figure shows the typical heat flux oscillations for single tube in the domain (second complete tube in Fig. 2 a). Graph (a) in Fig. 7 shows the comparison of SAS and *k*-ω SST models in geometry B (3D). SAS predicts a slightly lower mean and standard deviation for the heat flux compared to *k*-ω SST. The fluctuations, however, have nearly same oscillation period and the flow fields are visually very similar.

Graph (b) in Fig. 7 shows the results for *k*-ω SST and RSM-ω for geometry C (2D). The Reynolds Stress model predicts slightly lower average heat flux and its standard deviation. With this geometry, the heat flux and force oscillations are more complicated and have multiple characteristic frequencies. Both turbulence models predict the high standard deviation of $\langle q \rangle \approx 2$ kW/m^2 for this geometry, and the FFT signals are similar with both models. No significant differences between these models are observed.

Finally, graph (c) in Fig. 7 compares the *k*-ω SST and RSM- LPε for geometry E (2D). The RSM-LPε model predicts significantly lower heat transfer rate and standard deviation. The remarkable difference is that the RSM-LPε model shows nearly perfect periodicity in the solution, while the *k*-ω SST has more chaotic heat transfer signal. The RSM-LPε has also been tested in different tube bank geometries and similar periodicity prevails. The model predicts systematically lower heat transfer rates compared to *k*-ω SST, especially for the compact tube bank geometries (see Fig. 9). This indicates that the model is not suitable for complex boundary layer simulations, especially so in the compact geometries where the boundary layers become even more dominant part of the flow field.

Fig. 8 compares the temperature fields of *k*-ω SST and RSM- LPε for geometry B during one flow oscillation period. One flow oscillation period results in two heat transfer peaks shown in Fig. 7, as the flow attaches on the tube surface once from both sides of the tube. The different behaviour of the models in the boundary layer can be clearly identified in Fig. 8. The *k*-ω SST model results in more complex vortex structures after flow separation and the flow field is overall more nonlinear.

The turbulence model comparison concludes that the best turbulence models for the present application are the models adopting the *k*-ω formulation of Wilcox [20] for the boundary layer. The SAS, *k*-ω SST and RSM-ω all use this formulation and give very similar results for the heat transfer and flow field behaviour. The RSM-LPε cannot accurately predict the complex boundary layer phenomena and underpredicts the heat transfer rate especially in more compact geometries. This is most probably characteristic also for other ε-based turbulence models, such as the different *k*-ε models.

Comparison to Heat Transfer Correlations

The simulation results for the mean Nusselt number of different tube bank geometries are compared with the heat transfer correlations in Table 4. The numerical results are calculated with the *k*-ω SST model. All results are presented in the Nusselt number form of Gnielinski [2], Eq. (1). The correlation of Martin [3] is only valid for the transverse pitch ratios $a \leq 3$. Therefore, its values are only presented for the compact tube banks (geometries D and E).

The comparison in Table 4 shows that the CFD results are remarkably close to the correlation of Gnielinski. The maximum difference occurs with the largest transverse pitch ratio $a = 7.2$, for which the Gnielinski correlation predicts 13% smaller Nusselt number than the CFD simulation. For all other geometries, the Nusselt numbers are within ±8%. The additional simulation with smaller tube diameter of 44.5 mm in Geometry C agrees very well with the Gnielinski correlation as well.

The correlation of Zukauskas [1] predicts generally higher Nusselt numbers compared to Gnielinski [2] and CFD results, especially with increasing transverse pitch ratio a. The Nusselt numbers are nearly constantly 15% above the ones from CFD. Good agreement between the Martin correlation and CFD results is obtained for the compact tube bank geometries D and E.

It is concluded that the CFD heat transfer results agree very well with the available correlations. The results give additional reliability for the correlation of Gnielinski in the large transverse pitch ratio range ($a > 3$) where very little experimental or numerical data is available for comparison. The good agreement provides additional confidence for the correlation to be used in dimensioning, modeling and optimization of superheaters.

Fig. 9 gives a graphical summary of the CFD and correlation comparison. The Nusselt numbers of Zukauskas and Gnielinski are plotted as a function of transverse pitch ratio a for tube

diameter $D = 63.5$ mm and free channel velocity $U_\infty = 5$ m/s. Three different longitudinal pitches b are shown for the Gnielinski correlation, whereas b has no influence in the Zukauskas results. The figure shows the similar trend of *k*-ω SST results and Gnielinski correlation, which deviate only at the very high range of a. The figure also demonstrates the low Nusselt numbers of the RSM-LPε turbulence model, compared to the correlations and *k*-ω SST CFD results.

Comparison of Flow Oscillations in Different Geometries

Fig. 10 shows the typical oscillations of heat flux, drag force and lift force for a tube in geometry B and $\mathrm{Re}_{\Psi,l} = 5690$. The heat flux and drag force oscillate at the same frequency. The maximum heat flux coincides with the maximum drag. The lift force oscillates at half of the frequency of drag and heat flux. One oscillation period is visualized in Fig. 8, where the maximum lift occurs at the time $t = 2T/6$ and reaches minimum at $t = 5T/6$.

Fig. 11 shows typical lift oscillations for a tube in geometries C and D. The lift oscillations can cause tube vibrations in the transverse direction of the flow. Thus, the frequency must not coincide with the natural frequency of the tube bank geometry or with the acoustic frequencies of the flow channel. Fig. 11 displays the Fourier spectra for each signal in order to identify the dominant vortex shedding frequencies f_s. For geometry D, the lift oscillations have a single dominant frequency of 18.35 Hz. Single frequency is also characteristic for geometries A, D and E. For geometry C, the lift oscillations are more complicated and two dominant frequencies are identified as seen in Fig. 11. Multiple frequencies can possibly have a higher tendency for generating acoustic noise or tube vibrations. In addition, geometry C has a larger mean drag coefficient compared to other geometries, as shown in Table 5. The different behavior is associated with smaller tube diameter and larger longitudinal spacing compared to the other geometries. A similar trend was observed in the numerical study of Liang et al. [10]; drag steeply increases with increasing longitudinal pitch ratio b.

The dominant frequency of lift oscillations f_s can be used for calculating the Strouhal number $\mathrm{St} = f_s D/U_g$ for each geometry, as shown in Table 5. The numerical values are in the range that can be found in the experimental Strouhal number chart of Ziada [9] (St = 0.04-0.2). This indicates that the URANS simulations can be useful in analyzing the vortex shedding frequencies in tube banks. No experimental data could be found for the exact configurations simulated in this work and no definitive conclusions on the accuracy can be drawn. In any case, the unsteady simulations conducted in this work have demonstrated the ability of URANS simulations to reveal, at least qualitatively, interesting differences between the different tube bank configurations.

The mean drag coefficient, standard deviation of drag and standard deviation of lift coefficient are reported in Table 5. The mean lift was essentially zero for all geometries. It is notable, that the 3D simulations for geometry B with SAS and *k*-ω SST predict lower force oscillations compared to the 2D simulation with *k*-ω SST. Similar trend was observed in the previous section for heat flux oscillations. This indicates that for accurate prediction of the fluctuations, a 3D domain is required. It is very interesting to note that the Strouhal number and mean drag with *k*-ω SST are nearly the same in 2D and 3D simulations. Despite of the discrepancies in force oscillation amplitudes, the 2D simulations are able to predict the mean heat flux and forces, as well as Strouhal number comparable to 3D simulation. Iaccarino et al. [16] have reported similar results for flow across a square cylinder. In their 2D simulation, the experimental Strouhal number and mean drag coefficient was well predicted with the $v^2 - f$ URANS turbulence model. The evident trend is that 2D simulations overestimate the oscillation amplitudes of heat flux and forces, but are able to predict the mean values relatively well compared to 3D simulations. The turbulence model, on the other hand, has larger effect on the mean values than the domain

dimensions, as lower drag and Strouhal number are predicted by 3D SAS compared to 3D *k-ω* SST. In further studies, the results of URANS simulations should be compared to LES for better understanding of the accuracy of different RANS turbulence models.

CONCLUSIONS

A CFD based approach for predicting heat transfer and flow characteristics of inline tube banks with large transverse spacing is presented. The studied geometries, Reynolds numbers and gas properties are chosen relevant for power plant superheaters. In simulation domain study, it is shown that a periodic domain of five tubes predicts the average Nusselt number for the tube bank similar to a large domain of 144 tubes. Symmetry boundary conditions at domain sides are not recommended for small simulation domains as they prevent flow oscillations and underpredict the heat transfer rate.

The turbulence model comparison shows that the *k-ω* SST, RSM-*ω* and SAS give comparable heat transfer results, whereas the RSM-LP*ε* systematically underpredicts the heat transfer rate. For this reason, the turbulence models adopting the *k-ω* formulation of Wilcox [20] for the boundary layer are recommended. The numerical results of *k-ω* SST model are compared with the available heat transfer correlations, agreeing within ±13% with the correlation of Gnielinski for all analyzed tube bank geometries. The results give additional reliability for the correlation in superheater dimensioning in the large transverse pitch ratio range ($a > 3$), where little experimental or numerical data is available for comparison.

An interesting results is that 2D simulation domain is able to predict the mean heat transfer rate, drag coefficient and Strouhal number comparable to 3D simulations, but the force oscillation amplitudes are overpredicted. Therefore, a 3D domain is recommended for accurate force

predictions, but 2D simulations can provide fast estimations for the mean heat transfer and Strouhal number.

The presented CFD approach with suitable simulation domain and turbulence models is shown to give valuable information regarding the flow oscillations and heat transfer in inline tube banks with large transverse spacing. The promising results obtained by the URANS simulations are especially valuable from an industrial point of view, as LES modeling is still too time consuming for fast-paced industrial design purposes.

NOMENCLATURE

A	Surface area, m^2
a	Transverse pitch ratio of tube bank ($= S_T/D$), dimensionless
b	Longitudinal pitch ratio of tube bank ($= S_L/D$), dimensionless
C	Constant in Zukauskas correlation [1], dimensionless
C_D	Drag coefficient ($= F_D/(0.5\rho U_g^2 DL)$), dimensionless
C_L	Lift coefficient ($= F_L/(0.5\rho U_g^2 DL)$), dimensionless
c_p	Specific heat capacity, $J.kg^{-1}K^{-1}$
CFD	Computational Fluid Dynamics
D	Tube diameter, m
F_D	Drag force, N
F_L	Lift force, N
f_s	Vortex shedding frequency determined from lift oscillations, Hz
$f_{A,inline}$	Arrangement factor in Gnielinski correlation [2], dimensionless
FFT	Fast Fourier Transform
Hg	Hagen number ($= (\xi/2)\ \mathrm{Re}_{U_g,D}^2$), dimensionless
h	Convective heat transfer coefficient, $W.\ m^{-2}K^{-1}$
k	Thermal conductivity, $W.\ m^{-1}K^{-1}$
k	Turbulent kinetic energy, $m^2.s^{-2}$
L	Tube length, m
Lq	Leveque number in Martin correlation [3], dimensionless
l	Streamed tube length ($= \pi D/2$), m
LES	Large Eddy Simulation

m	Constant in Zukauskas correlation [1], dimensionless
$\mathrm{Nu}_{\mathrm{lam}}$	Laminar part of Nusselt number for flow across cylinder, dimensionless
$\mathrm{Nu}_{\mathrm{turb}}$	Turbulent part of Nusselt number for flow across cylinder, dimensionless
$\overline{\mathrm{Nu}_l}$	Tube bank mean Nusselt number based on l ($= \bar{h}l/k$), dimensionless
$\overline{\mathrm{Nu}_D}$	Tube bank mean Nusselt number based on D ($= \bar{h}D/k$), dimensionless
Pr	Prandtl number, dimensionless
Pr_s	Prandtl number at tube surface temperature, dimensionless
$\dot{Q}$	Heat transfer rate, W
q	Heat flux, W.m^{-2}
$\mathrm{Re}_{\Psi,l}$	Reynolds number based on Ψ and l ($= U_\infty l/\Psi\nu$), dimensionless
$\mathrm{Re}_{U_g,D}$	Reynolds number based on U_g and D ($= U_g D/\nu$), dimensionless
RANS	Reynolds-Averaged Navier-Stokes
RSM	Reynolds Stress Model
St	Strouhal number ($= f_s D/U_g$), dimensionless
S_L	Longitudinal tube spacing, m
S_T	Transverse tube spacing, m
SAS	Scale Adaptive Simulation
SST	Shear Stress Transport
T	Oscillation period, s
T_g	Flue gas mean inlet temperature, K
T_s	Tube surface temperature, K
ΔT_{lm}	Logarithmic mean temperature difference, K
t	Time, s
U_g	Gap velocity in tube bank ($= S_T U_\infty/(S_T - D)$), m.s^{-1}
U_∞	Free channel velocity before tube bank, m.s^{-1}
URANS	Unsteady Reynolds-Averaged Navier-Stokes
$\bar{X}$	Time-average value of variable X, various
$\langle X \rangle$	Standard deviation of time-varying variable X, various
y^+	Distance to the wall, dimensionless
Greek Symbols	
μ	Dynamic viscosity, kg.m^{-1}s^{-1}
ν	Kinematic viscosity, m^2.s^{-1}
ξ	Darcy-Weisbach friction factor, dimensionless
ρ	Density, kg.m^{-3}
τ	Normalized flow time ($= t/t_{end}$, where t_{end} is the end time), dimensionless
Ψ	Void fraction of tube bank ($= 1 - \pi/(4a)$), dimensionless
ω	Specific dissipation rate of turbulent kinetic energy, s^{-1}

REFERENCES

[1] A. Zukauskas, "Heat Transfer from Tubes in Crossflow", *Advances in Heat Transfer*, vol. 8, no. 1, pp. 93-160, 1972. DOI: 10.1016/S0065-2717(08)70038-8.

[2] V. Gnielinski, "Equations for calculating heat transfer in single tube rows and banks of tubes in transverse flow", *International Journal of Chemical Engineering*, vol. 19, no. 3, pp. 380–390, 1979.

[3] H. Martin, "The Generalized Leveque equation and its practical use for the prediction of heat and mass transfer rates from pressure drop", *Chemical Engineering Science*, vol. 57, no. 16, pp. 3217-3223, 2002. DOI: 10.1016/S0009-2509(02)00194-X.

[4] D. Taler, M. Trojan, P. Dzierwa, K. Kaczmarskib, and J. Taler, "Numerical simulation of convective superheaters in steam boilers", *International Journal of Thermal Sciences*, vol. 129, pp. 320-333, Jul. 2018. DOI: 10.1016/j.ijthermalsci.2018.03.005.

[5] D. Taler, M. Trojan, and J. Taler, "Mathematical modeling of cross-flow tube heat exchangers with a complex flow arrangement", *Heat Transfer Engineering*, vol. 35, no. 14-15, pp. 1334-1343, 2014. DOI: 10.1080/01457632.2013.876874

[6] C. Schuhbauer, M. Angerer, H. Spliethoff, F. Kluger, and H. Tschaffon, "Coupled simulation of a tangentially hard coal fired 700 °C boiler", *Fuel*, vol. 122, pp. 149-163, Apr. 2014. DOI: 10.1016/j.fuel.2014.01.032.

[7] Y. N. Chen, "Flow-induced vibration and noise in tube-bank heat exchangers due to von Karman streets", *ASME J. Eng. Ind.*, vol. 90, no. 1, pp. 134-146, Feb. 1968.

[8] G. J. Rae, and J. S. Wharmby, "Strouhal numbers for inline tube arrays", in: *Proceedings of the International Conference on Flow Induced Vibrations*, Bowness-on-Windermere, England, vol. 1, no. 1, pp. 233-242, 1987.

[9] S. Ziada, "Vorticity shedding and acoustic resonance in tube bundles", *Journal of the Brazilian Society of Mechanical Sciences and Engineering*, vol. 28, no. 2, pp. 186-189, 2006. DOI: 10.1590/S1678-58782006000200008.

[10] C. Liang, G. Papadakis, and X. Luo, "Effect of tube spacing on the vortex shedding characteristics of laminar flow past an inline tube array: A numerical study", *Computers and Fluids*, vol. 38, no. 4, pp. 950-964, 2009. DOI: 10.1016/j.compfluid.2008.10.005.

[11] X. Li, X. Wu, and S. He, "Numerical investigation of the turbulent cross flow and heat transfer in a wall bounded tube bundle", *International Journal of Thermal Sciences*, vol. 75, pp. 127-139, Jan. 2014. DOI: 10.1016/j.ijthermalsci.2013.08.001.

[12] N. Abed, and I. Afgan, "A CFD study of flow quantities and heat transfer by changing a vertical to diameter ratio and horizontal to diameter ratio in inline tube banks using URANS turbulence models", *International Communications in Heat and Mass Transfer*, vol. 89, pp.18-30, Dec. 2017. DOI: 10.1016/j.icheatmasstransfer.2017.09.015.

[13] K. Lam, and L. Zou, "Experimental study and Large Eddy Simulation for the turbulent flow around four cylinders in an in-line square configuration", *International Journal of Heat and Fluid Flow*, vol. 30, no. 2, pp. 276-285, Apr. 2009. DOI: 10.1016/j.ijheatfluidflow.2009.01.005.

[14] Y. A. Hassan, and H. R. Barsamian, "Tube bundle flows with the large eddy simulation technique in curvilinear coordinates", *International Journal of Heat and Mass Transfer*, vol. 47, no. 14-16, pp. 3057-3071, Jul. 2004. DOI: 10.1016/j.ijheatmasstransfer.2004.02.026.

[15] M. Salinas-Vázquez, M. A. De la Lama, W. Vicente, and E. Martínez, "Large Eddy Simulation of a flow through circular tube bundle", *Applied Mathematical Modelling*, vol. 35, no. 9, pp. 4393-4406, Sep. 2011. DOI: 10.1016/j.apm.2011.03.003.

[16] G. Iaccarino, A. Ooi, P. A. Durbin, and M. Behnia, "Reynolds averaged simulation of unsteady separated flow", *International Journal of Heat and Fluid Flow*, vol. 24, no. 2, pp. 147-156, Apr. 2003. DOI: 10.1016/S0142-727X(02)00210-2.

[17] M. Elkhoury, "Assessment of turbulence models for the simulation of turbulent flows past bluff bodies", *Journal of Wind Engineering and Industrial Aerodynamics*, vol. 154, pp. 10-20, Jul. 2016. DOI: 10.1016/j.jweia.2016.03.011.

[18] ANSYS FLUENT Theory Guide, Release 15.0, *ANSYS Inc.*, Canonsburg, Pennsylvania, 2013.

[19] C. J. Greenshields, Openfoam User Guide, vol. 3, no. 1, *OpenFOAM Foundation Ltd*, PO Box 56676, London, United Kingdom, 2011.

[20] D. C. Wilcox, "Turbulence Modeling for CFD", *DCW Industries Inc.*, La Canada, California, Jan. 1998.

[21] P. Stephan *et al.*, *VDI Heat Atlas*, 2nd edition, Springer-Verlag, Berlin, Heidelberg, 2010.

[22] T. L. Bergman, F. P. Incropera, D. P. DeWitt, and A. S. Lavine, *Fundamentals of Heat and Mass Transfer*, 6th edition, John Wiley & Sons, Hoboken, New Jersey, 2011.

[23] E. S. Gaddis, and V. Gnielinski, "Pressure drop in cross flow across tube bundles", *International Journal of Chemical Engineering*, vol. 25, no. 1, pp. 1–15, Jan. 1985.

[24] R. K. Shah, and D. P. Sekulic, *Fundamentals of Heat Exchanger Design*, John Wiley & Sons, Hoboken, New Jersey, 2003.

[25] V. Maakala, M. Järvinen, and V. Vuorinen, "Computational fluid dynamics modeling and experimental validation of heat transfer and fluid flow in the recovery boiler superheater region", *Applied Thermal Engineering*, vol. 139, pp. 222-238, Jul. 2018. DOI: 10.1016/j.applthermaleng.2018.04.084.

[26] A. Leppänen, H. Tran, R. Taipale, E. Välimäki, and A. Oksanen, "Numerical modeling of fine particle and deposit formation in a recovery boiler", *Fuel*, vol. 129, pp. 45-53, Aug. 2014. DOI: 10.1016/j.fuel.2014.03.046.

[27] S. Benhamadouche, and D. Laurence, "LES, coarse LES, and transient RANS comparisons on the flow across a tube bundle", *Int. J. Heat Fluid Flow*, vol. 24, no. 4, pp. 470-479, Aug. 2003. DOI: 10.1016/S0142-727X(03)00060-2.

Table 1 Mesh independence study for geometry B and $\mathbf{Re}_{\psi,l} = 5690$, first cell $y^+ \approx 1$ in all meshes

2D Periodic domain (5 tubes), *k-ω* SST	**Mesh 1**	**Mesh 2**	**Mesh 3**
# of cells	14 000	24 000	80 000
$\overline{\mathrm{Nu}_l}$	62.3	63.0	64.0
%-difference of $\overline{\mathrm{Nu}_l}$ to finest mesh	-2.7 %	-1.7 %	-
3D Periodic domain (5 tubes), SAS	**Mesh 1**	**Mesh 2**	
# of cells	380 000	800 000	
$\overline{\mathrm{Nu}_l}$	58.3	59.3	
%-difference of $\overline{\mathrm{Nu}_l}$ to finest mesh	-1.7	-	
2D Large domain (144 tubes), *k-ω* SST	**Mesh 1**	**Mesh 2**	
# of cells	530 000	1 570 000	
$\overline{\mathrm{Nu}_l}$	57.8	58.8	
%-difference of $\overline{\mathrm{Nu}_l}$ to finest mesh	-1.7 %	-	

Table 2 Values used in CFD simulations and heat transfer correlations

Property	**Value**
Flue gas mean inlet temperature, T_g (K)	914
Tube surface temperature, T_s (K)	612
Flue gas density, ρ (kg/m^3)	0.365
Specific heat, c_p (J/kg.K)	1302
Dynamic viscosity, μ (kg/m.s)	3.84e-5
Thermal conductivity, k (W/m.K)	0.064
Prandtl number at T_g, Pr (-)	0.78
Prandtl number at T_s, Pr$_s$ (-)	0.76

Table 3 Heat transfer correlations analyzed in this work

Correlation	Main equations for tube bundle Nusselt number	Validity range
Gnielinski [2]	$\overline{\mathrm{Nu}_l} = f_{A,inline}\left(0.3 + \sqrt{\mathrm{Nu}_{\mathrm{lam}}^2 + \mathrm{Nu}_{\mathrm{turb}}^2}\right)$ $f_{A,inline} = 1 + \frac{0.7(b/a - 0.3)}{\Psi^{1.5}(b/a + 0.7)^2}$ $\mathrm{Nu}_{\mathrm{lam}} = 0.664\mathrm{Re}_{\Psi,l}^{1/2}\mathrm{Pr}^{1/3}$ $\mathrm{Nu}_{\mathrm{turb}} = \frac{0.037\mathrm{Re}_{\Psi,l}^{0.8}\mathrm{Pr}}{1 + 2.443\mathrm{Re}_{\Psi,l}^{-0.1}(\mathrm{Pr}^{2/3} - 1)}$	$10 < \mathrm{Re}_{\Psi,l} < 10^6$ $0.6 < \mathrm{Pr} < 1000$ $b \geq 1.2$ Correction factor for less than 10 tube rows
Zukauskas [1]	$\overline{\mathrm{Nu}_\mathrm{D}} = C\mathrm{Re}_{U_g,D}^m\mathrm{Pr}^{0.36}\left(\frac{\mathrm{Pr}}{\mathrm{Pr_s}}\right)^{1/4}$ $\left.\begin{matrix} C = 0.27 \\ m = 0.63 \end{matrix}\right\}$ for inline tube bank and $\mathrm{Re}_{U_g,D}$ range $U_g = \frac{S_T U_\infty}{S_T - D}$ $\mathrm{Re}_{U_g,D} = \frac{U_g D}{\nu}$	$10^3 \leq \mathrm{Re}_{U_g,D} \leq 2 \cdot 10^5$ Other C and m values for different $\mathrm{Re}_{U_g,D}$ ranges. $0.7 < \mathrm{Pr} < 500$ $a \leq 3$ Correction factor for less than 16 tube rows
Martin [3]	$\overline{\mathrm{Nu}_D} = 0.404\mathrm{Lq}^{1/3}\left(\frac{\mathrm{Re}_{U_g,D} + 1}{\mathrm{Re}_{U_g,D} + 1000}\right)^{0.1}$ $\mathrm{Lq} = 1.18\mathrm{HgPr}\frac{(4a/\pi - 1)}{b}$ $\mathrm{Hg} = (\xi/2)\,\mathrm{Re}_{U_g,D}^2$ from pressure drop correlation of Gaddis and Gnielinski [23]	$1 < \mathrm{Re}_{U_g,D} < 2 \cdot 10^6$ $0.7 < \mathrm{Pr} < 700$ $1.02 \leq a \leq 3$ $b \leq 3$ Additional term for less than 10 tube rows

Table 4 Comparison of CFD results (*k-ω* SST) and heat transfer correlations. The percentage difference for correlation compared to CFD shown in parenthesis. Correlation of Martin is valid only for compact tube banks

Geometry	D (mm)	a (-)	b (-)	$\mathrm{Re}_{\psi,l}$ (-)	$\overline{\mathrm{Nu}}_l$ CFD	$\overline{\mathrm{Nu}}_l$ Gnielinski [2]	$\overline{\mathrm{Nu}}_l$ Zukauskas [1]	$\overline{\mathrm{Nu}}_l$ Martin [3]
A (2D)	63.5	7.20	1.50	5300	58.0	50.7 (-13%)	66.9 (+15%)	-
B (3D)	63.5	4.80	1.50	5700	61.9	58.7 (-5%)	71.7 (+16%)	-
B (3D)	63.5	4.80	1.50	4500	53.5	51.1 (-4%)	60.9 (+14%)	-
C (2D)	44.5	6.85	2.70	3800	48.3	48.5 (+0%)	54.7 (+13%)	-
D (2D)	63.5	3.15	1.89	6300	70.3	73.8 (+5%)	78.8 (+12%)	75.2 (+7%)
E (2D)	63.5	1.89	1.89	8100	92.1	99.5 (+8%)	99.5 (+8%)	93.6 (+2%)

Table 5 Strouhal number, mean drag coefficient, and standard deviations of drag and lift coefficients for the simulated geometries. Results calculated with 2D domains and *k-ω* SST turbulence model, but 3D results are also shown for geometry B

Geometry	St from simulations	Mean drag coefficient $\overline{C_D}$ (-)	Standard deviation of drag $\langle C_D \rangle$	Standard deviation of lift $\langle C_L \rangle$
A	0.13	0.42	0.66	0.92
B	0.10 (SAS, 3D)	0.33 (SAS, 3D)	0.38 (SAS, 3D)	0.69 (SAS, 3D)
	0.12 (*k-ω* SST, 3D)	0.45 (*k-ω* SST, 3D)	0.47 (*k-ω* SST, 3D)	0.78 (*k-ω* SST, 3D)
	0.12 (*k-ω* SST, 2D)	0.46 (*k-ω* SST, 2D)	0.68 (*k-ω* SST, 2D)	0.98 (*k-ω* SST, 2D)
	0.10 (large domain)	0.33 (large domain)	0.49 (large domain)	0.66 (large domain)
C	0.19 and 0.06	0.79	0.78	0.89
D	0.16	0.39	0.35	1.00
E	0.14	0.38	0.34	0.92

List of figure captions

Figure 1 Tube bank geometries analyzed in CFD simulations

Figure 2 (a) 3D simulation domain with 380 000 hexahedral cells. Periodic boundary conditions are used in all domain boundaries. (b) Large 2D simulation domain with 144 tubes. The domain sides are periodic, inlet has constant velocity and outlet has constant pressure boundary condition

Figure 3 Comparison of 2D and 3D calculation domains (left) and periodic and symmetry boundary conditions (right) in terms of typical heat flux oscillations of single tube. Average and standard deviation calculated from longer flow period than presented in figure

Figure 4 Left: Instantaneous 3D vortex structures determined by Q-criterion and colored by Z-velocity. Right: Local instantaneous heat flux at tube surface, demonstrating the 3D nature of the flow field. Periodic domain is repeated once to display two columns of tubes, SAS turbulence model

Figure 5 Instantaneous temperature field for the large domain of geometry B (144 tubes, 2D). Graph below shows the time-average heat flux for each tube row. The mean Nusselt number for the tube bundle is 58.8

Figure 6 Heat flux signal of a single tube as a function of time and its Fourier transform. Top: tube in row 6 of the large domain. Middle: tube in row 19 of the large domain. Bottom: Tube in the small periodic simulation domain

Figure 7 Comparison of turbulence models in terms of typical heat flux oscillations for single pipe in different tube bank geometries. Average and standard deviation calculated from longer flow period than presented in figure

Figure 8 Temperature field during one lift oscillation period in geometry B (3D) and $\mathrm{Re}_{\Psi,l} = 4500$, k-ω SST and RSM-LPε models. The models result in different boundary layer behavior, k-ω SST characterized by more vortical flow field

Figure 9 Comparison of CFD results with correlations of Zukauskas [1] and Gnielinski [2]. Results of k-ω SST agree remarkably well with Gnielinski, whereas RSM-LPε underestimates the Nusselt number

Figure 10 Typical oscillations of heat flux, drag and lift for tube in geometry B (3D) and $\mathrm{Re}_{\Psi,l} = 5690$, SAS turbulence model. Heat flux and drag oscillate at same frequency, and at twice the frequency of lift

Figure 11 Lift coefficient C_L and its Fourier spectra for geometries D (top) and C (bottom)

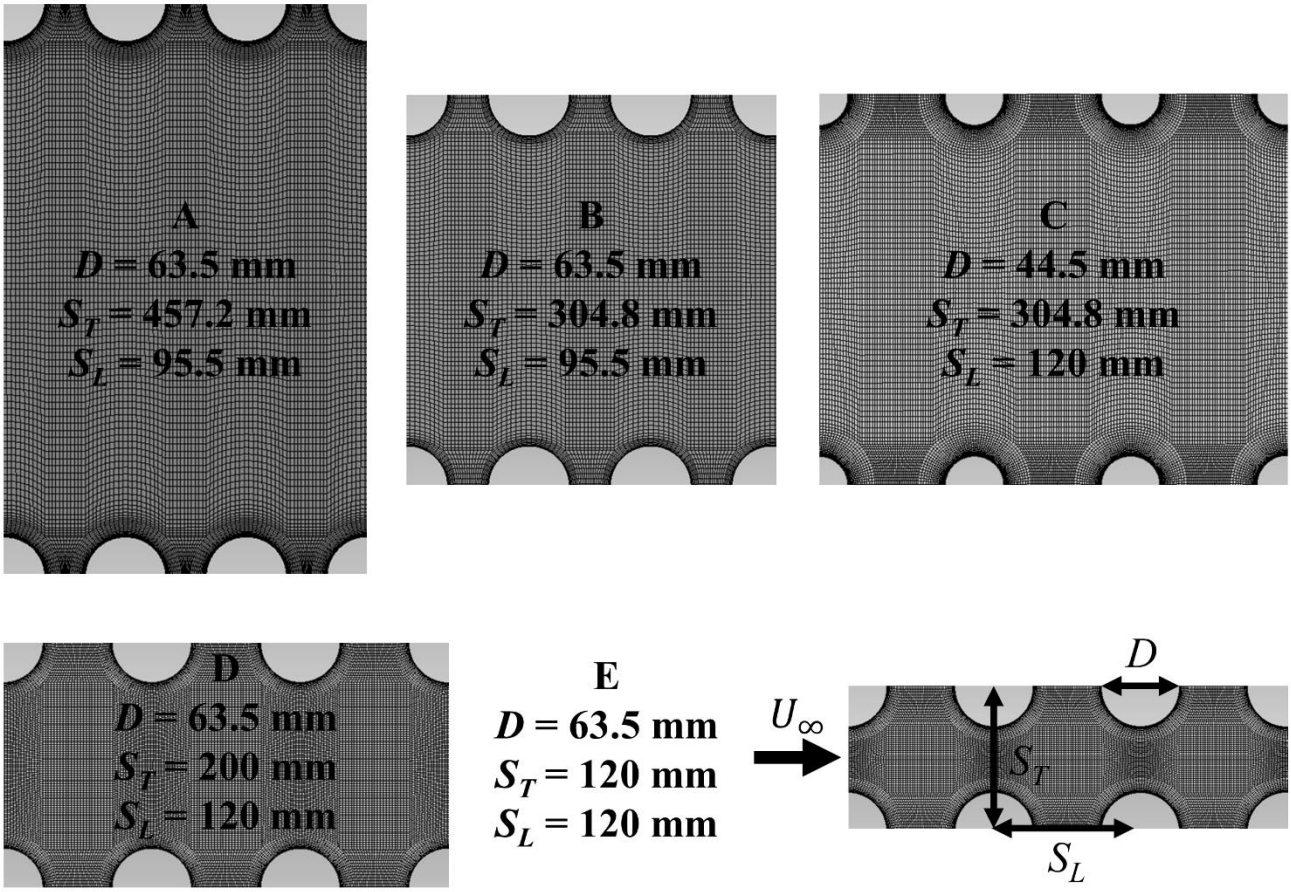

Figure 1 Tube bank geometries analyzed in CFD simulations

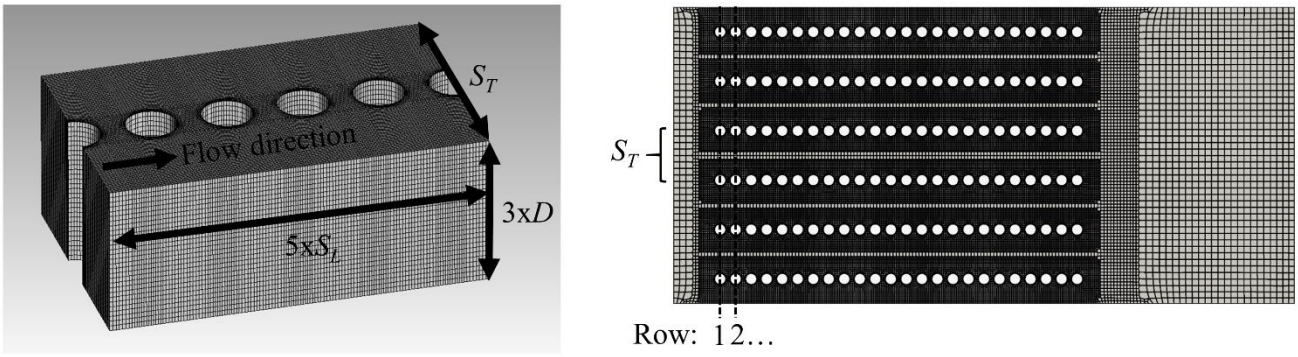

(a) Small periodic domain, 3D (b) Large domain of 144 tubes, 2D

Figure 2 (a) 3D simulation domain with 380 000 hexahedral cells. Periodic boundary conditions are used in all domain boundaries. (b) Large 2D simulation domain with 144 tubes. The domain sides are periodic, inlet has constant velocity and outlet has constant pressure boundary condition

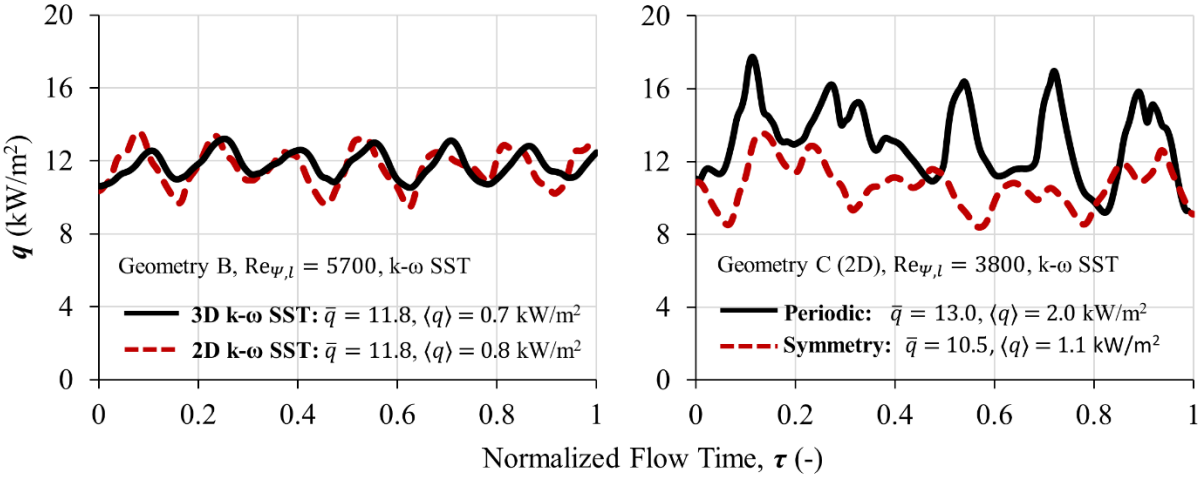

Figure 3 Comparison of 2D and 3D calculation domains (left) and periodic and symmetry boundary conditions (right) in terms of typical heat flux oscillations of single tube. Average and standard deviation calculated from longer flow period than presented in figure

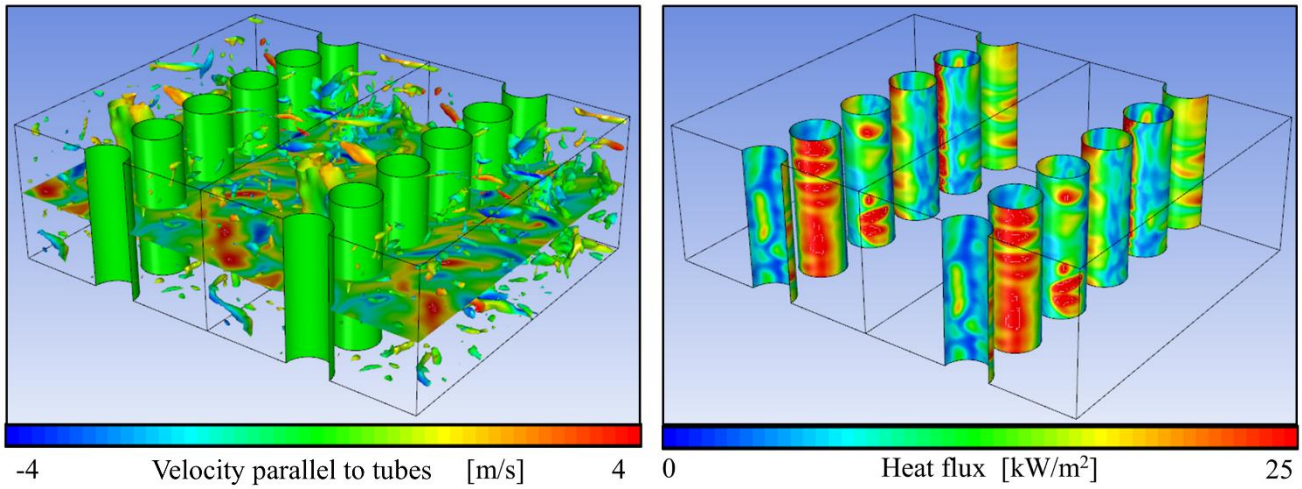

Figure 4 Left: Instantaneous 3D vortex structures determined by Q-criterion and colored by Z-velocity. Right: Local instantaneous heat flux at tube surface, demonstrating the 3D nature of the flow field. Periodic domain is repeated once to display two columns of tubes, SAS turbulence model

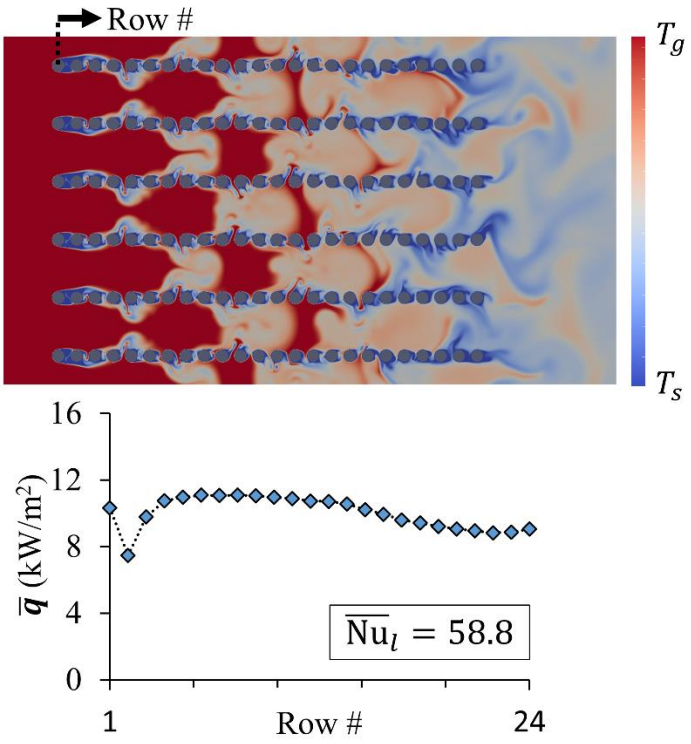

Figure 5 Instantaneous temperature field for the large domain of geometry B (144 tubes, 2D). Graph below shows the time-average heat flux for each tube row. The mean Nusselt number for the tube bundle is 58.8

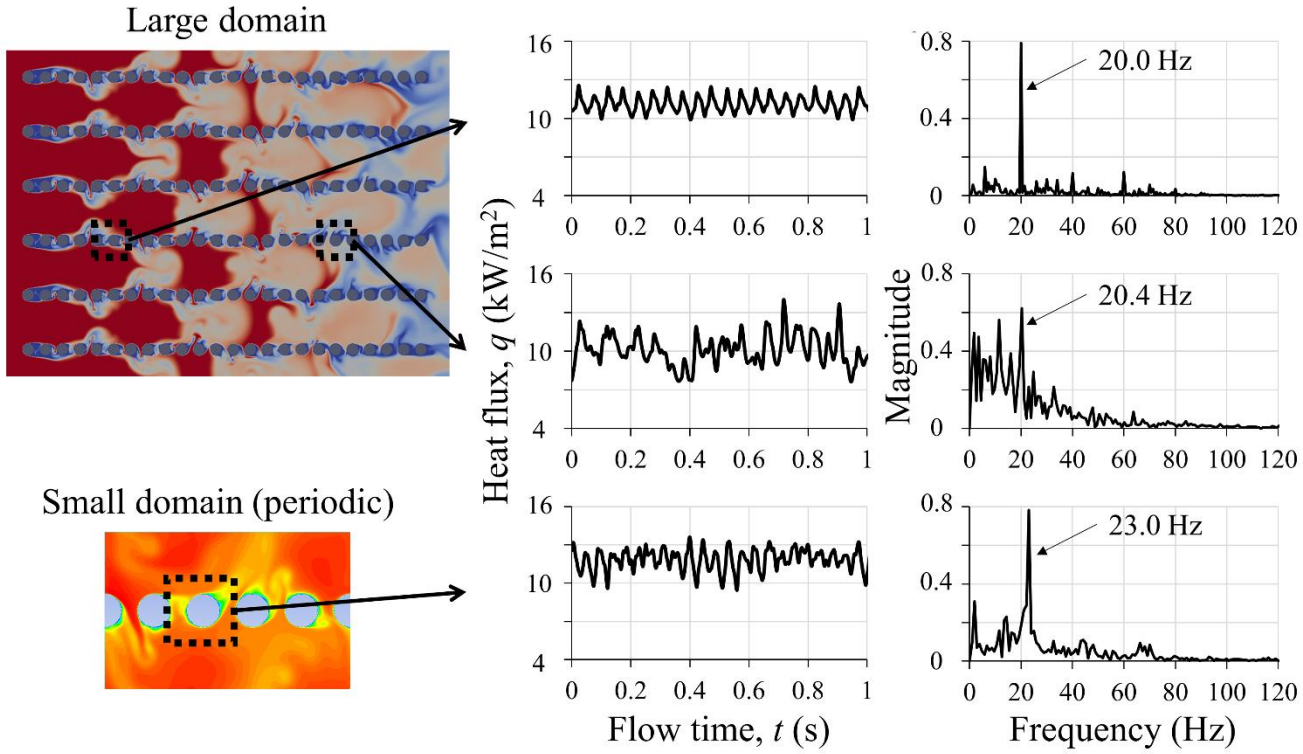

Figure 6 Heat flux signal of a single tube as a function of time and its Fourier transform. Top: tube in row 6 of the large domain. Middle: tube in row 19 of the large domain. Bottom: Tube in the small periodic simulation domain

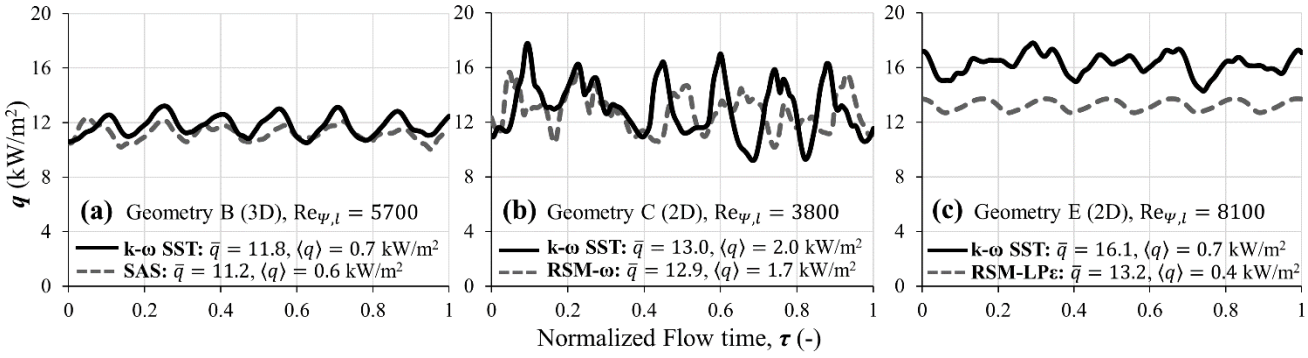

Figure 7 Comparison of turbulence models in terms of typical heat flux oscillations for single pipe in different tube bank geometries. Average and standard deviation calculated from longer flow period than presented in figure

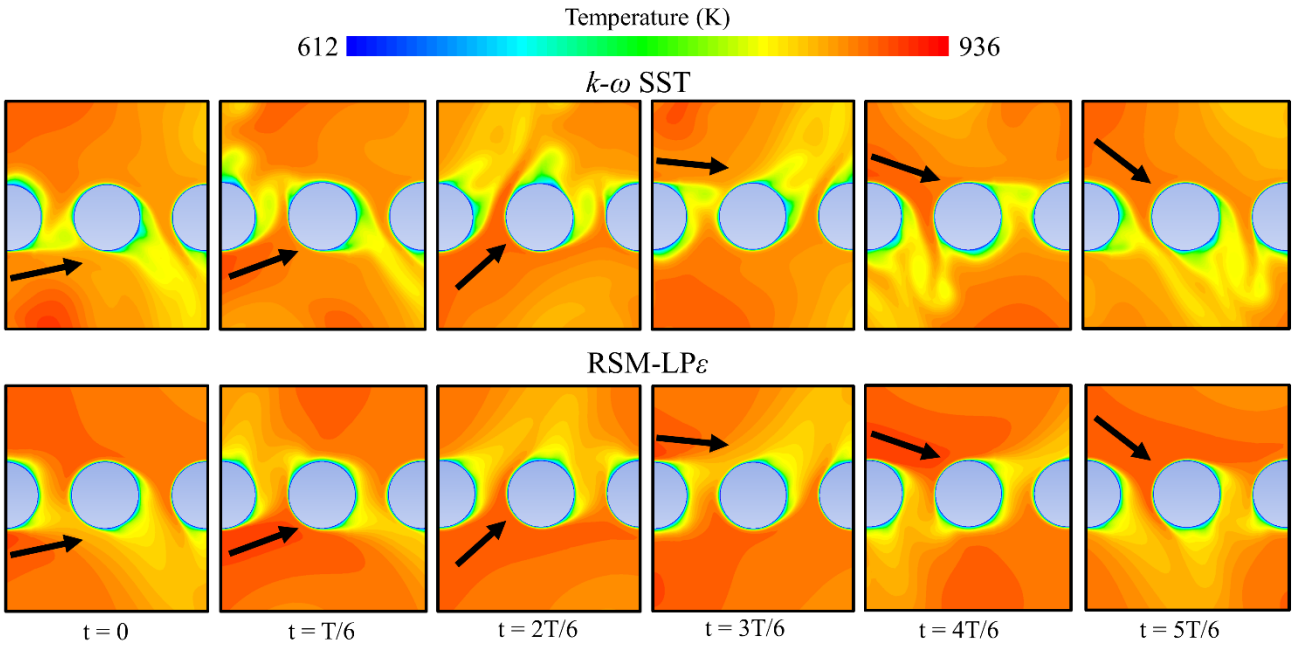

Figure 8 Temperature field during one lift oscillation period in geometry B (3D) and $\mathbf{Re}_{\Psi,l} = 4500$, *k-ω* SST and RSM-LP$\varepsilon$ models. The models result in different boundary layer behavior, *k-ω* SST characterized by more vortical flow field

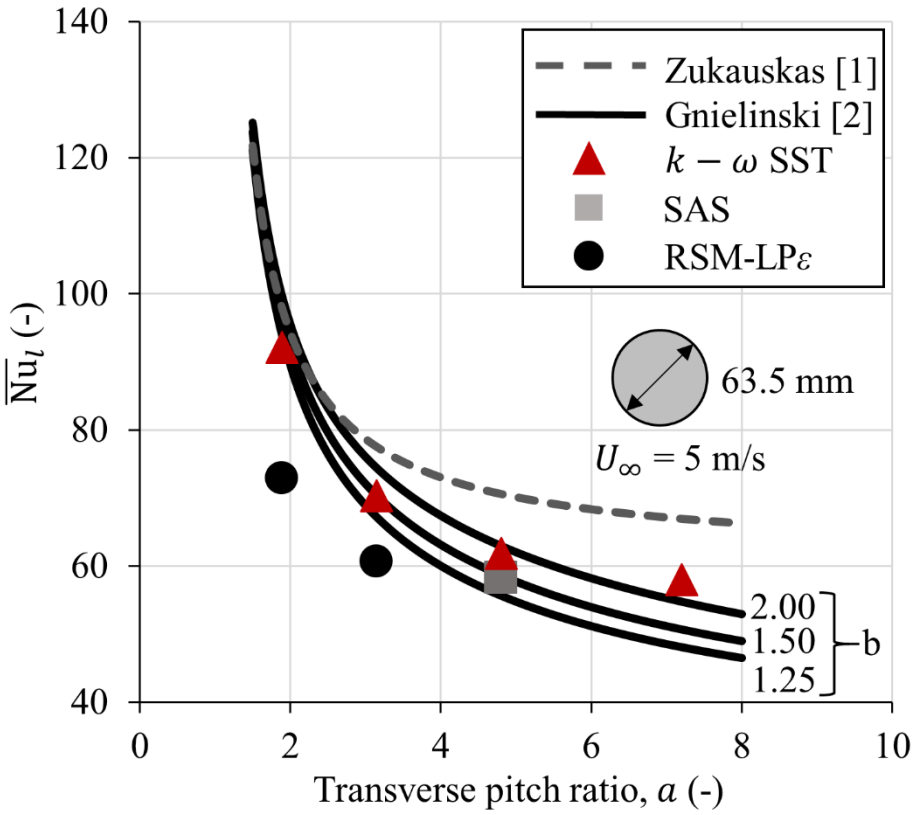

Figure 9 Comparison of CFD results with correlations of Zukauskas [1] and Gnielinski [2]. Results of *k-ω* SST agree remarkably well with Gnielinski, whereas RSM-LP*ε* underestimates the Nusselt number

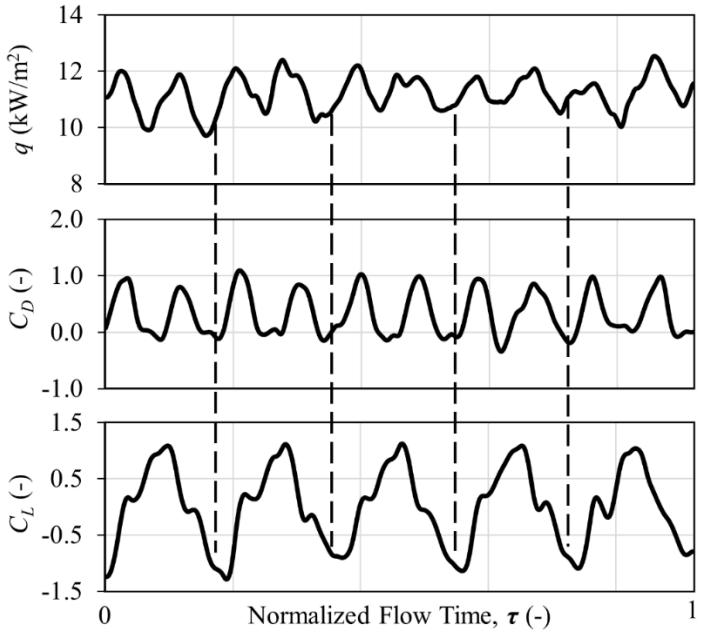

Figure 10 Typical oscillations of heat flux, drag and lift for tube in geometry B (3D) and $\mathbf{Re}_{\psi,l} = \mathbf{5690}$, SAS turbulence model. Heat flux and drag oscillate at same frequency, and at twice the frequency of lift

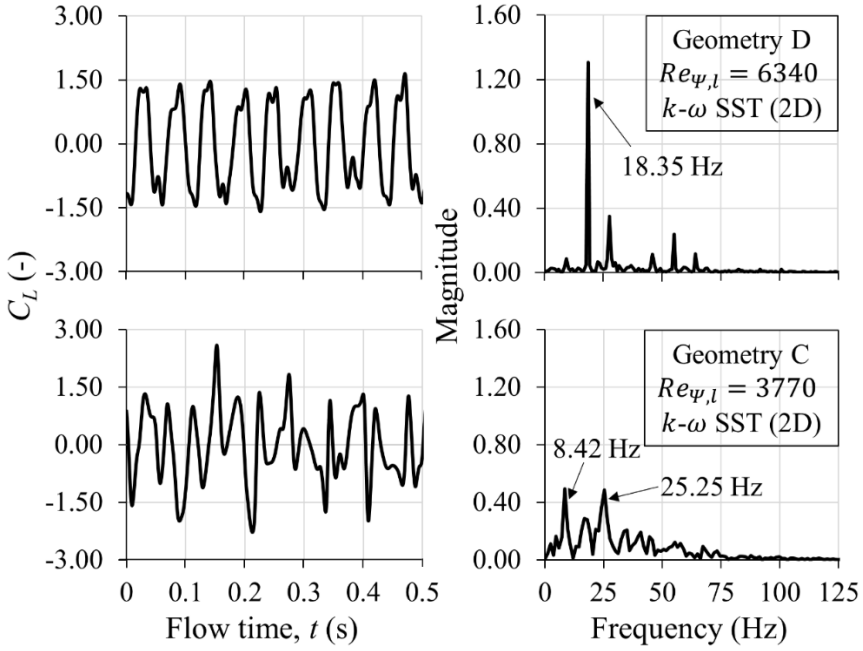

Figure 11 Lift coefficient C_L and its Fourier spectra for geometries D (top) and C (bottom)

Niko Niemelä is a Ph.D. student at the Tampere University (TAU), Finland. He majored in Fluid Dynamics and Combustion in his M.Sc. degree and he currently conducts research related to CFD modeling of biomass combustion. He teaches reactive flows and numerical modeling.

Antti Mikkonen is a Ph.D. student at the Department of Civil Engineering, Tampere University, Finland. His main research considers impinging jet heat transfer in glass tempering. He also teaches CFD.

Kaj Lampio has just completed his Ph.D. thesis defense of "Optimization of Fin Arrays Cooled by Forced or Natural Convection". He has long experience in teaching fluid dynamics and heat transfer at the Tampere University, Finland.

Jukka Konttinen is a Professor of Chemistry of Biorefining at the unit of Materials Science and Environmental Engineering of Tampere University (TAU), Finland. His fields of research and education are related to thermochemical conversion (biorefining) of biomass and wastes, renewable energy and related environmental technologies. Both experimental and modeling.